Real-Time damage localization by means of MEMS sensors and use of wireless data transmission

Masanobu Shinozuka[1]*, Chulsung Park[2], Pai H. Chou[2] and Yoshio Fukuda[1],
[1]Department of Civil and Environmental Engineering, University of California Irvine
[2] Department of Electrical Engineering and Computer Science, University of California, Irvine
Irvine, CA 92612, USA

ABSTRACT

When lifeline systems such as water delivery networks are damaged, it is critical to pinpoint the location of the damage, to assess the extent of the damage, and to mitigate the damage in real-time. We propose a wireless sensor network consisting of densely populated, optimally located MEMS sensors that monitor pipe pressure and transmitting data wirelessly. Transient analysis of water pressure in the networked pipes showed that the damage sustained by the pipe creates a state of transient in the pipe pressure, which is detectable by MEMS sensors for damage localization and estimation. This is critical information to enhance post-event disaster mitigation.

Keywords: Damage detection, Assessment, Lifeline system, MEMS sensor, Wireless transmission.

1. INTRODUCTION

Urban water delivery network systems, particularly the underground components such as pipeline networks, can be damaged due to earthquakes, pipe corrosion, severely cold weather, heavy traffic load on the ground surface, and many other man-made or natural causes. In all these situations, the damage can be disastrous: water leakage at high pressure may threaten the safety of near-by buildings due to scouring of their foundations; flooding could create major traffic congestion if the pipe ruptures under a busy street; and above all, after a severe earthquake, pipe damage may result in reduction in the water head, thus degrading post-earthquake firefighting capability of the community, while at the same time force the human consumption of water to drop below an acceptably low level. Yet, the current technology is not capable of accurately detecting the location and assessing the extent of these damages easily or quickly, especially immediately after a major damaging event. As a result, even if full resources are available, failure to locate, assess, and mitigate the damages will still lead to widespread human miseries, inconveniences, and outbreak of diseases after a major catastrophic event.

These observations, particularly those related to severe earthquakes, strongly suggest that we urgently need rapid, and preferably real-time, damage detection and assessment technologies in order to reduce the negative societal impact of disruption to lifeline systems, such as water delivery systems, resulting from pipe breaks and other damages..

2. RELATED WORK

In recent years, real-time damage assessment and diagnosis of buried pipelines has attracted much attention from researchers focusing on establishing the relationship between damage ratio (breaks per unit length of pipe) and ground motion, taking the soil condition into consideration (Nishio [1], Takada [2], Yamazaki [3]). Eguchi [4] put forward a method in which nominal damage estimated through some earthquake parameters is updated gradually based on the collection of post-earthquake observation information. Shinozuka [5] developed a methodology to detect the damage location and severity with the aid of neural network methods, and applied the method to a water network that consisted

Nonintrusive Inspection, Structures Monitoring, and Smart Systems for Homeland Security,
edited by Aaron A. Diaz, H. Felix Wu, Steven R. Doctor, Yoseph Bar-Cohen,
Proc. of SPIE Vol. 6178, 61780A, (2006) · 0277-786X/06/$15 · doi: 10.1117/12.659084

of 31 nodes and 50 pipes. However, real water networks consist of a much larger number of nodes and links in a more complex topology. To address these difficulties, the methodology consists of three significant phases, in the first phase, the water pressure distribution patterns are computed for the damaged network by means of forward analysis, with the aid of hydraulic analysis code. The results are visualized using Geographic Information Systems (GIS) mapping. In the second phase, the correlation values between the water pressure distribution patterns are computed. A damage index is defined and evaluated for all the pipes on the basis of these correlation values. Finally, the inverse analysis is carried out to identify the possible damage locations and severity.

3. PROPOSED DAMAGE INDENTIFICATION METHODOLOGY

In this section, we describe our proposed damage identification methodology, called MEMS-Sensor/Wireless Transmission (MSWT). The main difference with the Water Head Gradient-Based methodology is that ours measures the acceleration change of the water delivery network and is non-invasive, as shown in Figure 1. We use MEMS sensor for measurement and wireless transmission to enable real-time monitoring and damage localization. To accurately locate the damage at a reasonable cost over a vast lifeline network, we support adjustable monitoring granularity through trade-offs among deployment density, sensor accuracy, wireless communication range, and costs. We also discuss required features for the wireless sensor nodes, which will be described in Section 4.

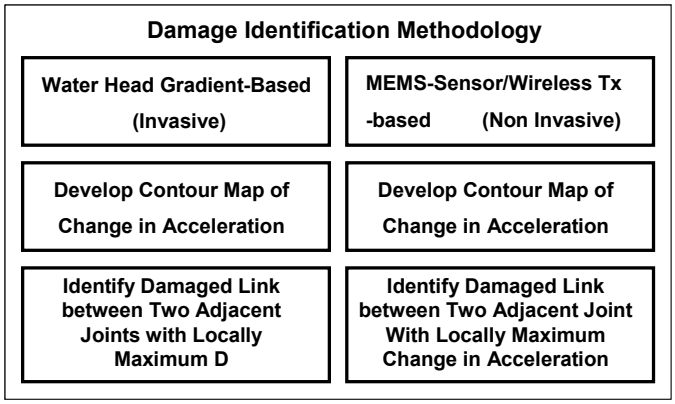

Figure 1. Comparison of Water Head Gradient -Based and Change in Acceleration-Based

3.1 Non-Invasive Detection

While invasive methodologies prevail in conventional monitoring systems such as MLGW's water system [8], our non-invasive detection methodology has many advantages, in terms of cost and effectiveness. First, our non-invasive methodology mainly relies on local acceleration change on the surface of a water pipe. This means our monitoring system can be installed on existing water delivery networks at low installation cost without requiring modifications to the water pipes. This translates into not only substantially lower installation cost but also enhances maintainability over invasive methodologies. In addition, recent advances in MEMS technology have resulted in a variety low-cost, low-power, miniature accelerometers at different levels of performance. Table 1 shows the specifications of several MEMS accelerometers, which differ in terms of the acceleration range, the number of axes, sensitivity, bandwidth, size, power consumption, and price. The variety of MEMS accelerometers enables system designers to select the right sensor according to the system level requirements such as power, size, and coverage of each sensor. By choosing the right type

of MEMS accelerometer for the right context, we will be able to develop a more cost-effective monitoring system than conventional ones.

Table 1. Specifications of MEMS Accelerometers

Part Name	Acce. Range (g)	Axis	Sensitivity (mV/g)	Freq. (HZ)	Size (mm)	Power (mW)	Price ($)
SD1221(Silicon Designs)	±2	One	2000	0 ~ 400	9x9x3	50	130
H34C(Hitach Metals)	±3	Three	333	0 ~ 100	3.4x3.7x0.9	1	9.8
MMA7260Q (Freescale)	±1.5	Three	800	0 ~ 150	6x6x1.5	2	5.67
ADXL202(AnalogDevice)	±2	Two	375	0 ~ 6K	5x5x2	1.8	12.6
KXM52-1050(Kionix)	±2	Three	660	0 ~ 3K	5x5x1.8	5	100

Adjustable Monitoring Granularity

The monitoring granularity determines the number of points to be monitored in order to locate damage in the water delivery network. The more points we monitor (i.e., finer spatial granularity, up to a practical limit), the more precisely we can locate the damage, but it also increases the installation and maintenance cost. Therefore, a good monitoring system should be designed to operate effectively for a wide range of spatial granularity, to be determined by users at deployment time.

The monitoring granularity in turn depends on two hardware parameters: the sensitivity of the MEMS sensor and the radio range of the wireless interface. For coarse-grain monitoring, we may need more sensitive sensors and a longer-range wireless interface for a single sensor node to cover the same area of the water delivery network. On the other hand, for finer-grain monitoring, the system may use MEMS with lower sensitivity and radios with a shorter range.

To fully address these design issues, we designed two types of wireless sensor nodes that can communicate each other. The first is called Eco, which has a short-range radio and a lower-sensitivity MEMS accelerometer. The second is called DuraNode, which has a longer-range radio and three highly sensitive accelerometers. The detailed specifications of these two sensor nodes are presented in the next section. By forming a heterogeneous wireless monitoring network using these two types of nodes, we can easily adapt the spatial granularity of the monitoring system to the specific deployment site.

Real-Time Monitoring

Increasing demand for fast damage detection and assessment necessitates real-time monitoring capabilities. Real-time monitoring poses many challenges to designing sensor nodes, including fast communication links, fair and efficient media access protocols (MAC), and low-latency routing protocols. In our monitoring system, we use two different wireless interfaces. For short range communication, the Eco node uses a 2.4GHz custom radio with a data rate of 1Mbps. For longer range communication, DuraNode uses the 802.11b WiFi interface, whose maximum data rate is 11Mbps. Also, Eco and DuraNode use Time Division Multiple Access (TDMA) and 802.11b MAC, respectively, as their MAC protocol. Comparing with other wireless sensor platforms such as MICA2 [9], Telos[10], and Stargate[11], our Eco and DuraNode have higher or equivalent radio performance of in terms of maximum bit rate and radio range when used with the proper antenna [12],[13].

4. WIRELESS SENSOR NODES DESIGN

We have designed and implemented two types of wireless sensor nodes, called Eco and DuraNode, to support the proposed real-time monitoring damage localization methodology. Although both of them can collect tri-axial acceleration data and transmit wirelessly, Eco and DuraNode are totally different platforms with complementary features, as shown in Table 2. Eco is ultra-compact, low power, low cost, and is suitable for dense deployment with a short wireless range. In contrast, DuraNode is equipped with three high-end, high-accuracy accelerometers and a long range wireless interface (802.11b), in addition to the same type of radio as Eco. At the same time, DuraNode consumes over ten times the power as Eco. We take advantage of their characteristics and deploy a mix of these two types of sensor nodes by adapting the choice to the specific requirements on the spatial granularity of the water delivery network. Two sensor nodes can communicate each other via the available 2.4GHz wireless radio or RS232 serial interface. This combination is expected to make the proposed real-time monitoring methodology accurate and cost effective.

Table 2. Comparison of Eco and DuraNode

	Eco	**DuraNode**
Size (mm)	13 x 11 x 8	140 x 80 x 20
Sensor	One H34C	Three SD1221, Gyroscope
Power Consumption (mW)	Max. 100	Max. 1000
Max. Air Data Rate (bps)	1M	11M
Battery	30mAh Li-Polymer	4000mAh Li-Ion
Wired Interface	Serial, SPI	Fast Ethernet, Optical
Wireless Interface	2.4GHz Custom Radio	WiFi / 2.4GHz Radio
Radio Range (m)	10 ~ 20	200 ~ 300
Cost ($) @ 1000	50	400

4.1 DuraNode

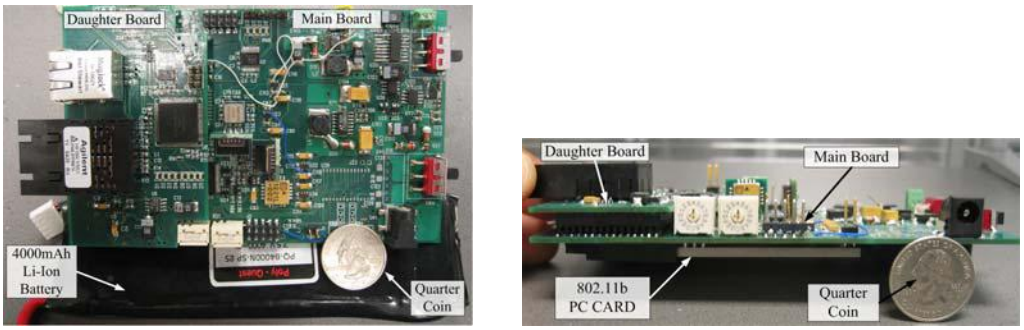

(a) Top View **(b) Side View**

Figure 2. Photos of DuraNode

Figure 2 shows the picture of the DuraNode hardware. It consists of two boards: main board and daughter board. The main board itself can be used as a wireless sensor node, and we call this stand alone operating mode wireless mode. As

shown in Figures 2 (a) and 3 (a), the main board has everything a wireless sensor node may need, including microcontrollers, sensors, and a wireless communication interface. On the other hand, the daughter board, as shown in Figure 2 (b), has only a microcontroller but two wired communication interfaces, namely Fast (10/100 Mbps) Ethernet and Optical. Another daughter card can provide the wireless link to a short-range network of Eco nodes. In addition, DuraNode can also use both wired and wireless interfaces in dual mode. As shown Figure 4, DuraNode consists of four subsystems: Microcontroller, Communication, Power, and Sensor.

A. Microcontroller Subsystem

As shown in gray color in Figure 4, the microcontroller subsystem consists of three low-power microcontrollers (two PIC18F8680s [4] and one MC9S12NE64 [5]), one asynchronous first-in first-out (FIFO) memory (CY7C Series), and one real-time clock (DS1284). The PIC18F8680 is an 8-bit microcontroller from Microchip with 3.3KB of RAM, 64KB flash memory, and an 8-channel 10-bit A/D converter. The MC9S12NE64 is a Freescale HSC12-based 16-bit microcontoller, which has an integrated Fast Ethernet MAC/PHY controller, 8KB RAM, and 64KB flash memory. We use a 28-pin PLCC socket for the FIFO memory, instead of soldering it directly onto the printed circuit board. This enables us to adjust the size of the FIFO memory according the required data latency and power management scheme. The memory size is selectable among 8KB, 16KB, 32KB, and 64KB. The RTC is used for time synchronization with a resolution of 1ms. Using these components, we implemented a dual microcontroller architecture. This architecture is unique to sensor nodes designs and enables us to achieve design goals including low-power, low jitter, and high network performance. The physical architecture, as shown in Figure 4, consists of three microcontrollers sharing a FIFO memory, an I2C bus, and interrupt signals for inter-processor communication. We can optimize power consumption in this architecture by first assigning tasks to the microcontrollers and then scale the microcontrollers' clock frequencies and supply voltages based on the timing constraints and the complexity of assigned tasks.

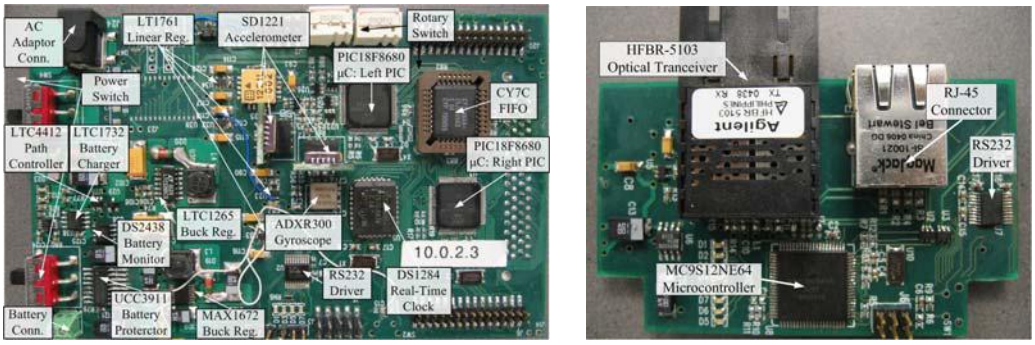

(a) Main Board **(b) Daughter Board**

Figure 3. Photos of Main Board and Daughter Board

B. Communication Subsystem

The communication subsystem, colored sky-blue in Figure 4, consists of an 802.11b wireless PC card (MA401), a Fast Ethernet controller (MC9S12NE64), and an optical transceiver (HFBR-5103). The bit rate, power consumption, and range of each communication interface are summarized in Table 2. Having multiple communication interfaces is very useful, especially for indoors deployment. LAN is available in most of buildings, and sometimes an optical network is also available especially along utility conduits. With the wired interface, DuraNode can easily tap into a pre-installed network instead of having to set up its own wireless network. For outdoors deployment, we can unplug the daughter board to save the power consumed by the wired interfaces. Also, DuraNode supports the soft transition between a wired and a wireless interface. When the micrcocontroller detects the sudden failure of the current communication interface, it automatically switches to the other interface within 10 microseconds.

C. Power Subsystem

The power subsystem, colored orange in Figure 4, consists of a set of regulators, a power path controller, battery-management ICs, and two power sources: a Li-Ion battery and an AC adapter. In designing the power system of battery-powered devices, the crucial issue is how to design the regulator topology, because it directly affects the overall power efficiency of the system. The inputs to designing the regulator topology can be each subsystem's supply voltages, current consumption levels, expected battery lifetime, and so on. The rightcolumn of Table 2 shows those of DuraNode. Based on this table, we designed DuraNode's regulator topology as shown in Figure 2. DuraNode has two switching regulators and four linear regulators, which are combined in a manner that maximizes the conversion efficiency and minimizes the cost and space. We used switching regulators for power-hungry subsystems such as 802.11b and Fast Ethernet, and for the rest of subsystems we used a two-stage conversion scheme. In this scheme, the switching regulator first converts a battery's output voltage (7.4V) into an intermediate voltage level (5.2V) and the linear regulators of each subsystem finally.

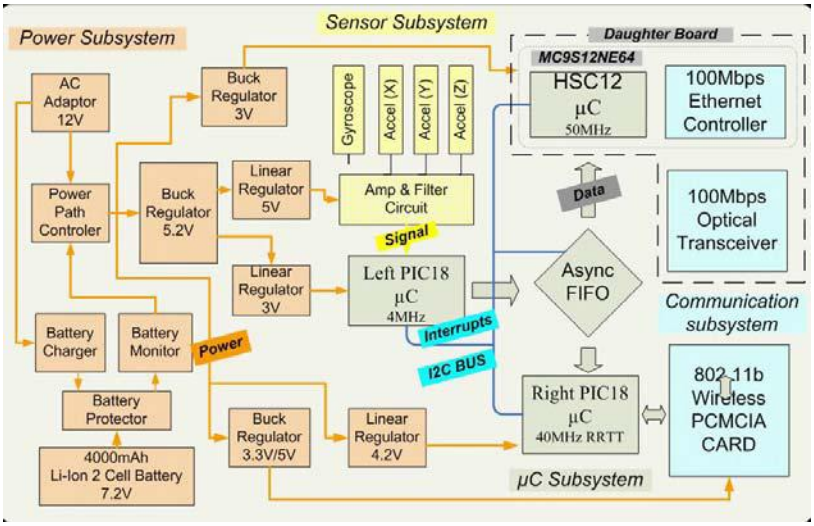

Figure 4. Block Diagram of . DuraNode

D. Sensor Subsystem

The sensor subsystem, colored yellow in Figure 4, consists of three accelerometers (SD1221) [6], one gyroscope (ADXRS300), and amplifier and filter circuitry. Three SD1221s are used to monitor tri-axial vibration.
The SD1221 is a low-noise integrated accelerometer whose input acceleration range is from -2g to +2g. Also, its frequency response range is 0 to 400 Hz. Two differential analog output signals (0.5 to 4.5V) of the SD1221 first go to the low-noise operational amplifier (LMV751), which converts these signals into a signal-ended one. Then, the signal flows through an RC filter and feeds the AD converter of the left microcontroller.

4.2 Eco

The Eco sensor node (Figure 5) consists of four subsystems:MCU/Radio, Sensors, Power, and expansion port.

A. MCU/Radio

The nRF24E1 is a 2.4GHz RF transceiver with an embedded 8051-compatible MCU (DW8051) [6]. The MCU has 512Byte ROM for a bootstrap loader, a 4KBRAM for the user program, SPI (3-wire), RS-232, and a 9-ch. ADC. The

ADC is software-configurable for 6--12 bits of resolution. A 32KB serial (SPI) EEPROM stores the application program. The nRF24E1's 2.4GHz transceiver uses a GFSK modulation scheme with 125 frequency channels that are 1MHz apart. The transmission output power is also software-configurable for four different levels: -20dBm, -10dBm, -5dBm, and

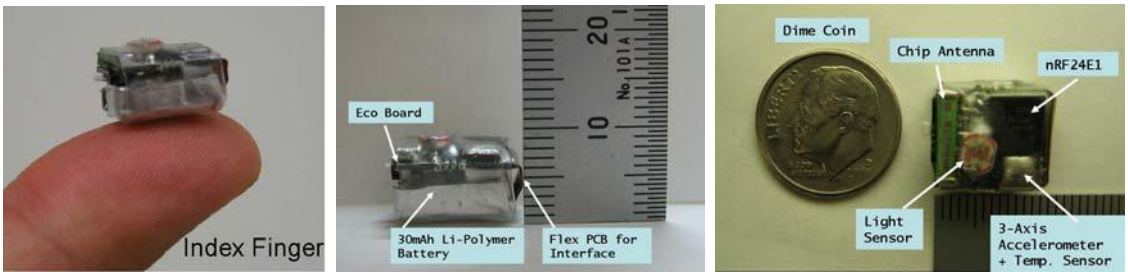

(a) On the finger **(b) Side View** **(c) Top View**

Figure 5. Photos of Eco Sensor Node

0dBm. The RainSun chip antenna (AN9520) measures 9.5mm(H)x 1.5mm(W) x 1mm(H) and has a maximum gain of 1.5dBi.Sensors Eco has a 3-axial acceleration sensor, Hitachi-Metal H34C (3.4mm x 3.7mm x 0.92mm). It measures acceleration from -3g to +3g and temperature from 0--75C while consuming 0.36mA at 3V in active mode. Eco also has a light sensor (S1087).

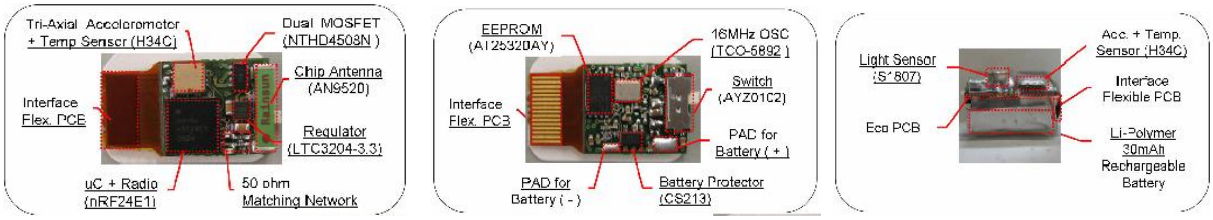

(a) Top View **(b) Bottom View** **(c) Side View**

Figure 5. Photos of Eco Sensor Node

B. Power

Eco's power subsystem includes a 3.3V regulator (LTC3204-3.3V), battery protection circuitry, and a custom 30mAh rechargeable Li-Polymer battery (12mm(L) x 10mm(W) x 5mm(H)). LTC3204 (2mm x 2mm) is a low noise regulated charge pump regulator that outputs 3.3V. Its maximum output current is 50mA and average efficiency over a Li-Polymer battery's output voltage range (3.0V to 4.2V) is 80% at Eco's maximum operating current. To measure the actual battery capacity, we continuously discharge it at constant 30mA and it lasts 1.5 hours. This translates into 45mAh.

C. Expansion Port

Eco's expansion port has 16 pins including 4 digital I/Os, one analog input, SPI, RS232, 3.3V output, and voltage input for a regulator and battery charging. This port enables Eco to interface with other sensing devices such an image sensor, gyroscope, pressure sensor, or compass. We can charge the battery and program the EEPROM via this expansion port.

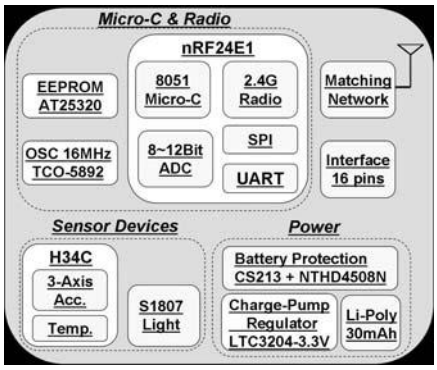

Figure 6. Block Diagram of Eco

5. PRELIMINARY EXPERIMENTS

To show the effectiveness of our MEMS sensor-based real-time monitoring system, we set up a small water delivery network using 1-inch diameter PVC pipes. We installed four DuraNodes onto the network and collected vibration data in real-time. This section describes the details of our experimental setup and presents the 3-axial vibration data collected under two different levels of water pressure.

5.1 Experimental Setup

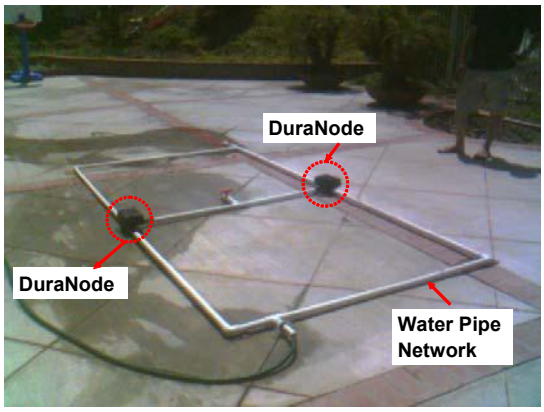

(a) Photo of Water Pipe Network.

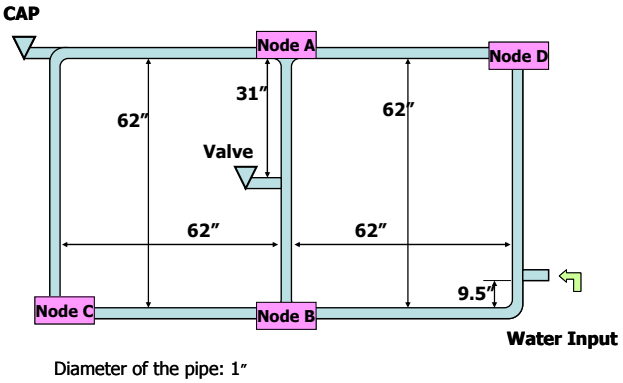

(b) Dimension of Water Pipe Network and locations where 4 DuraNodes are installed.

Figure 7. Experimental Setup

Our water delivery network consists of seven pieces of 62-inch PCV pipes (with a 1-inch diameter), one PCV pipe cap, and one valve. As show in Figure 7 (b), we construct a rectangular-like pipe network, whose lengths on the two sides are 124 inches and 62 inches. Also, one valve is installed in the middle of the network (marked as VALVE in Figure 7) and one cap (marked as CAP in Figure 7) on the top-left vertex of the network. In our experimental setup, the CAP functions as a possible damage in the pipe network. We can increase the water pressure inside the pipe network by injecting water at the WATER INPUT. At low water pressure, the CAP remains closed as it initially is. This status represents ``No Damage in the Network." However, when the pressure increases so that it is high enough to force the CAP open, the pipe network can be considered ``Damaged."

In the current experimental setup, four DuraNodes are installed onto the pipe network, as shown in Figure 7. They keep transmitting 3-axial vibration data to a host computer via an access point in real-time. The sampling rate is set to 1KHz.

The VALVE is used to vary the overall water pressure inside the pipe network. By manually setting the valve to three different states,(CLOSE, HALF-OPEN, OPEN), we can adjust the water pressure inside the pipe network. (HIGH, MEDIUM, LOW).

5.2 Results

The results are 3-axial vibration data from four DuraNodes. We start recording data when we start injecting water to the pipe network, and we stop when the CAP is forced to open. Also, we repeat the same experiment at various levels of water pressure (HIGH, MEDIUM, LOW) using the VALVE. In this section, we present only the X-axis vibration data in the high pressure condition (Figure 7). Each graph in Figure 1 shows the vibration data from each of the four DuraNodes labeled A, B, C, and D. The sudden and drastic change of vibration in each graph is caused by damage to the pipe network, which means that the CAP is forced open by high water pressure.

Upon closer examination of Figure 7, we find that the amplitude of each peak is different: Nodes A, B, C, and D have amplitudes of 0.5g, 0.65g, 0.35g, and 1.2g, respectively. These differences can be used to locate the damage in the pipe network. It is clear that the impact caused by the sudden opening of the CAP is attenuated as it travels through the pipe network. We can say that the amount of vibration change observed on a sensor node is near inversely proportional to the distance between the sensor node and the location of damage location. In this case, Node C must be located farthest from the location of damage, and that the damage happened near Nodes A, B, and D. Similar analysis will enable closer localization of the damage.

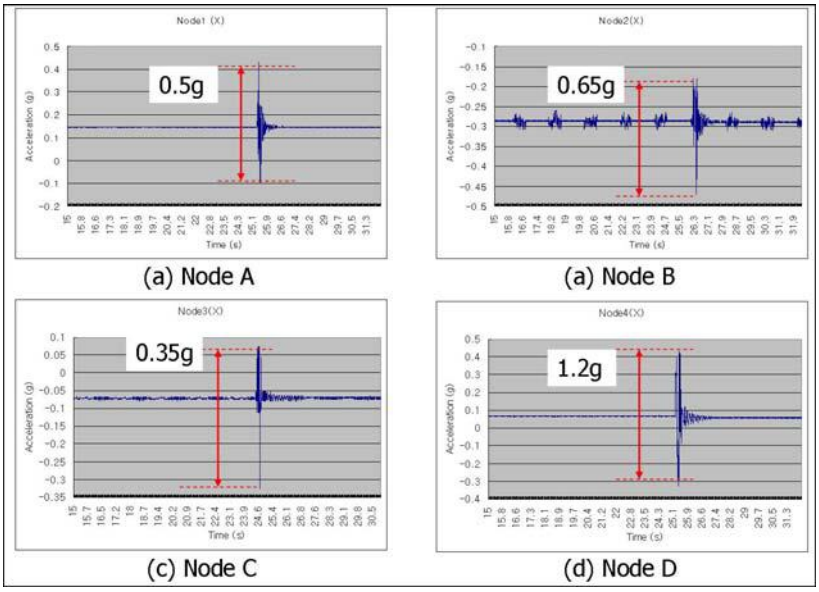

Figure 7. Acceleration Data of 4 DuraNode under High Pressure

5. FUTURE WORK

Our future work includes experiments on a water network that is larger in scale than one tested in our preliminary experiments described in Section 5. We plan to install our Ecos and DuraNodes on a subset of the Westminster network (Figure 8). This will be done in conjunction with existing SCADA measurement locations in the Westminster network.

The main technical challenge will be to install these sensor nodes on the pipe surface. Observing that there are a large number of hydrants in the Westminster system, it appears best to install them on the pipe at the hydrant locations as Mizushina [7] suggested.

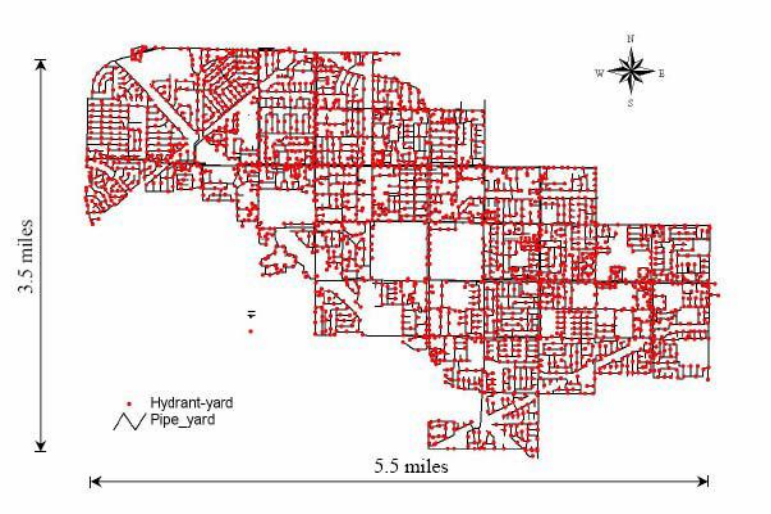

Figure 8. Hydrants and Pipes in Westminster Water System

7. CONCULSION

In this paper, we propose the MEMS-sensor/Wireless Transmission-based real-time monitoring system for a water delivery network. We present several advantages of our approach over conventional monitoring systems. First, our monitoring methodology is non-invasive. Second, our system enables real-time damage detection and location.
Third, we can build more cost-efficient monitoring system using the MEMS sensors and wireless transmission technologies. We also present our preliminary experiments conducted on a small pipe network. The experimental results demonstrate the feasibility of our approach in detecting and locating damages in the water delivery network. As our future work, we plan to conduct a larger-size experiment in Westminster Water System.

ACKNOWLEDGEMENTS

This study was done under National Science Foundation Grant # CMS 0509018 and Grant .# CMS 0112665. Their supports are immensely appreciated.

REFERENCES

[1] Nishio, N. (1994) "Damage Ratio Prediction for Buried Pipelines Based on the Deformability of Pipelines and the Nonuniformity of Ground ," J. of Pressure Vessel Technology, ASME, 116, 459-466.
[2] Tanaka, S., Shinozuka, M., and Hwang, H. H. M. (1993) "LIFELINE-W(2) User's Guide: a Program for Connectivity and Flow Analysis of a Water Delivery System Under Intact and Seismically Damaged Conditions." Technical Report, Princeton University.

[3] Yamazaki, F., Katayama, T., and Yoshikawa, Y. (1994) "On-Line Damage Assessment of City Gas Networks Based on Dense Earthquake Monitoring." Proc. 5th U.S. Conf. on Earthq. Engrg., EERI, Vol.4, 829-837.
[4] Eguchi, R. T., Chrostowski, J. D., and Tillman, C. W., (1994) "Early Post-Earthquake Damage Detection for Lifeline System." EQE Research Report prepared for National Science Foundation.
[5] Shinozuka, M., and Liang, J. (1999) "On-Line Earthquake Damage Identification of Water Supply Networks." Research Report, International Institute of Innovative Risk Reduction Research on Civil Infrastructure Systems, University of Southern California. (in print)
[6] Takada, S., and Ogawa, Y. (1994) "Seismic Monitoring and Real Time Damage Estimation for Lifelines." Proc. 4th U.S. Conf. on Lifeline Earthq. Engrg., ASCE, 224-231.
[7] Xuejiang Dong, Masanobu Shinozuka (2004), GIS-based seismic damage localization for water supply systems, 13th World Conference on Earthquake Engineering, Vancouver, Canada, August, 2005 Paper No.520
[8] MLGW's water system: http://www.mlgw.com
[9] MICA2: http://www.xbow.com/Products/productsdetails.aspx?sid=61
[10] Joseph Polastre, Robert Szewczyk, David Culler, The Fourth International Conference on Information Processing in Sensor Networks: Special track on Platform Tools and Design Methods for Network Embedded Sensors (IPSN/SPOTS), April 25-27, 2005
[11] Stargate: http://www.xbow.com/Products/Product_pdf_files/Wireless_pdf/6020-0049-01_B_STARGATE.pdf
[12] Chulsung Park and Pai H. Chou, "Eco: Ultra-Wearable and Expandable Wireless Sensor Platform," Proc. Third International Workshop on Body Sensor Networks, April 3-5, 2006. MIT Media Lab.
[13] Chulsung Park, Pai H. Chou, and Masanobu Shinozuka, "DuraNode: Wireless Networked Sensor for Structural Health Monitoring," to appear in Proceedings of The 4th IEEE International Conference on Sens, Irvine, CA, Oct. 31 - Nov. 1, 2005